Simulation of a 3D wall jet cooling of a glass plate oven partition

Rodrigo de Jesus Freire Neno
rodrigo.neno@tecnico.ulisboa.pt

Instituto Superior Técnico, Universidade de Lisboa, Portugal

June 2021

Abstract

The coil coating process plays a very relevant role in industry. The conventional process uses convective heat to evaporate the solvent. Instead, in this work radiative heat transfer is used to increase the process efficiency and reduce the carbon footprint. However, the radiative heat was provided by radiative burners and the configuration of the system considered uses a glass plate to avoid ignition of the solvent in the oven. This work is based on the thermal control of the window glass, which aims to guarantee the safety of the operation.

Window cooling by cold wall jets allows to remove heat from the medium. Different turbulence models are used in the numerical calculation of wall jets and are compared against available heat transfer correlations to select the most accurate one. Heat transfer correlations for the cold wall jets are numerically obtained for different cooling schemes.

The one-dimensional (1D) conduction-radiation model with discrete ordinates method is developed to predict the thermal behaviour of the window. The 1D model was developed for fast process characterization, accounts with the heat transfer correlations and provides an analysis of different cooling parameters (temperature, velocity, angle, scheme and others).

An optimization method provides the optimal cooling conditions to respect the safety requirements (maximum window temperature and thermal gradient). Finally, the 3D numerical simulations of the full curing furnace are performed including detailed effects which were not considered on the development of the 1D model.

Keywords: glass plate cooling, wall jets, radiation-conduction, numerical simulation, energy optimization

1. Introduction

The drying/curing process of a metal strip is a relevant process in the industry. This industrial process emerged on 1930's but had its high increase during the 90´s [1]. The process is based on the application of a pre-painted coating, that enters the oven and the energy is provided to drive the thermochemical process on the metal strip.

Recent studies are now focused on a change from a convective convectional oven process to a radiative exchange from infrared (IR) burners [2]. The change allows a higher efficiency of the coating process due to less energy demand because the evaporated solvent is used as fuel for the radiant burners [3]. The current work is devoted to an analysis of a radiative curing furnace, more specific, a glass partition inside the oven. The thermal control and analysis of the radiative participating medium is important to assure that the safety requirements are met.

The curing furnace for this process is composed by two coupled modules (sections). On the top, one section is dedicated to the generation of radiant heating (energy source for coating processing) – radiant burner section (RBS) – and on the bottom another section is devoted to the coating drying and curing processes – curing oven section (COS), both identified by the red and blue region in Figure 1, respectively.

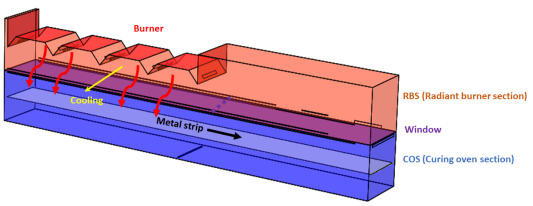

Figure 1: 3D model of radiative curing furnace.

The RBS is the upper section where the burners are placed on ceiling and provide the necessary radiative energy (red arrows in Figure 1) to coil coating on the lower section, where a metal strip is continuously fed. The two domains are separated by a

glass (see purple region in Figure 1). The window is the medium that makes the separation of the two environments, a crucial element for a proper operation. The window composed by an IR-transmissive material prevents the thermal decomposition of the solvent loaded atmosphere (COS) at high temperatures.

The window is a semi-participating medium to radiation and therefore absorbs part of that radiative energy. The magnitude of the temperature inside the window must be below the critical values of the material to avoid the development of thermally inducted mechanical stresses leading to the window structure fatal failure. The current work is focused on the modeling, simulation, analysis, and optimization of the glass oven partition.

A cooling system is a very important strategy used to remove heat from the window and therefore reduce the glass temperature. The cooling jet is injected parallel to the window by a cooling slot, in a transversely direction to the movement of the coil (see yellow curve in Figure 1). The wall jet faces a backward step at the injection and the flow develops until achieves the perpendicular wall at the end of the window. There are different cooling schemes which are possible to install, and are schematically represented in Figure 2. The red arrows represent the direction of the cooling injection from above the window (RBS) and the black arrows from underneath the window (COS).

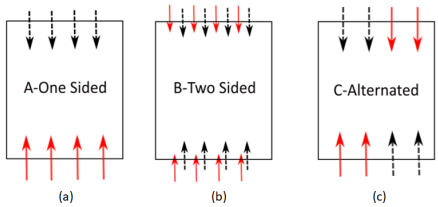

Figure 2: Representation of different cooling schemes in a top view: (a) Scheme A; (b) Scheme B; and (c) Scheme C. Red/black arrows indicate cooling direction from above/below the window.

The cooling system is enabled on both sections (RBS and COS) due to recirculation systems. An extraction port removes the flow from the environments, passes the fluid through an outside heat exchanger (HX) and then the cold flow is inserted again into the system from above and underneath the window. There are two different HX due to the different environments (RBS and COS). The energetic optimization of this work provides the optimal operating condition (reduced energy cost of the HX) respecting the safety requirements of the glass partition (maximum temperature and gradient inside the window). The optimization also dictates which is the most suitable cooling scheme.

2. Non-isothermal wall jet

This section intends to perform a validation study of the numerical error associated to simulation of wall jets. Wall jets started to be studied by Glauert [4], in mid 1950s, by deriving an analytical solution for laminar and turbulent jets. Launder and Rodi [5] made a review of those studies up to 1983, not only summarizing but including the Reynolds average turbulence modeling required, treating as two different layers, inner and outer layer.

The wall jet enters the domain with a certain velocity and develops along x, see Figure 3. The Reynolds number (ratio of inertial forces to viscous forces) is defined, specifically for wall jet, as:

$$Re_j = \frac{U_j \times b}{\nu} \tag{1}$$

where b (jet height) is defined as the characteristic length.

George [6] developed a theoretical study demonstrating that the profiles have a self-similar solution by an adequate inner and outer scaling. The theoretical study was corroborated and validated with other experimental studies [7, 8].

The heat transfer studies on this topic have received much lower attention than the isothermal case. Dacos [9] measured experimentally, temperature and heat fluxes for plane and curved wall jets with isothermal conditions and AbdulNour et al. [10] measured experimentally the convective heat transfer coefficients on the developing region, up to $x/b = 20$. Naqavi [11] completed a recent direct numerical simulation (DNS) study focused on the heat transfer of a wall jet up to $x/b = 40$. Other initial experimental studies show that at fully developed downstream locations, a correlation can be applied:

$$Nu = C \times Re^{0.8} \times \left(\frac{x}{b}\right)^{-0.6} \tag{2}$$

where C is a empirical coefficient varying from 0.071 [12] to 0.115 [13].

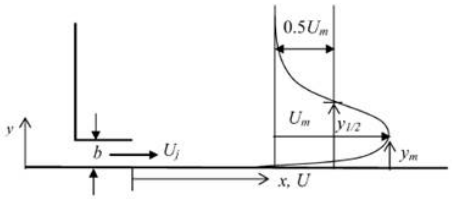

Figure 3: Wall jet nomenclature and representation, extracted from Reference [14].

The numerical simulations of wall jets were performed in a commercial software (ANSYS Fluent) by balance in mass, momentum, and total energy described by the continuity, the Navier-Stokes, and total energy equation in a time average formulation (RANS):

$$\frac{\partial(\rho v_i)}{\partial x_i} = 0 \tag{3}$$

$$\frac{\partial(\rho v_i v_j)}{\partial x_j} = \frac{\partial p}{\partial x_i} + \frac{\partial}{\partial x_j}\left[\mu\left(\frac{\partial v_i}{\partial x_j} + \frac{\partial v_j}{\partial x_i} - \frac{2}{3}\delta_{ij}\frac{\partial v_i}{\partial x_j}\right)\right] + \frac{\partial}{\partial x_j}\left(-\rho\overline{v_i' v_j'}\right) \tag{4}$$

$$\frac{\partial(\rho C_p v_i T)}{\partial x_i} = -\frac{\partial}{\partial x_i}(k_t \frac{\partial T}{\partial x_i}) + S_e \tag{5}$$

The Reynolds stresses ($-\rho\overline{u_i' u_j'}$) must be modeled. The transport equation for a scalar variable:

$$\rho\overline{u_j}\frac{\partial\overline{\phi}}{\partial x_j} - \frac{\partial}{\partial x_j}\left[\Gamma_{\phi,eff}\frac{\partial\overline{\phi}}{\partial x_j}\right] = S_\phi \tag{6}$$

where ϕ represents the species mass fractions as well the variables of turbulence models, $\Gamma_{\phi,eff}$ the effective diffusion coefficient, and S the source term of the equation. The following turbulence models within Fluent were considered for comparison and analysis:

- Standard $k-\epsilon$ model with standard, scalable, and non-equilibrium wall function (WF); and
- Realizable $k-\epsilon$ model with standard WF;

and the low-Reynolds models:

- $k-\epsilon$ low Reynolds Yang Shish, and AKN;
- $k-\omega$ SST (Menter); and
- Spalart-Allmaras (SA).

The no-slip boundary condition of the bottom wall influences the development of the turbulent boundary layer and provides steeper gradients of velocity near the wall. The modeling is influenced by its growth. The boundary layer region has been studied and subdivided into three different regions: the laminar sublayer ($y^+ < 5$), buffer region ($5 < y^+ < 20$), and the log-law region ($20 < y^+ < 0.1\delta$).

A mesh with the first cell placed inside the laminar sublayer is referred as low-Re modeling and the mesh should be refined enough as the first cell be at $y^+ < 1$ and several layers up to $y^+ < 5$. When the first cell is in the log-law region ($u^+ = 1/k \times \ln(y^+) + C^+$), at $y^+ > 20$, wall functions theory are applied in the standard high Re turbulence models.

The DNS study [11] was used as a basis to validate the models considered. The jet enters the domain at $Re_j = 7500$ from an inlet with height equal to 20 mm. The jet inlet temperature is constant and equal to 22ºC and develops streamwise along a no-slip isothermal wall at 44ºC. The computational domain has the dimensions of $50b$ and $40b$ in x and y directions, respectively. The remain normal wall ($x = 0$) at the injection provides the jet entrainment with a uniform flow at 0.06 U_j. The upper boundary ($y = 40b$) has a free slip boundary condition. The mesh grid varies in x and y direction with a ratio since the refinement near the injection and near the bottom surface is more relevant to simulate the behaviour of the jet.

The accuracy of the turbulence models depends on the capability to predict the behaviour near the wall, inside the boundary layer. Numerical simulations with high Reynolds turbulence models with wall functions require the first grid at $y^+ > 20$. The problem is that it requires a coarser mesh and the minimum admissible mesh becomes lower than 20 at middle of the domain and equal to 15 at the end of the domain. Simulations were performed by increasing the first cell size but that originated too low resolution inside the remain jet structure.

Figure 4 shows the growth rate of the flow along x, represented by the streamwise jet half width ($y_{1/2}$). Figure 4 compares the low-Re turbulence models with the DNS [11] and with the linear relationship proposed by Abrahamsson *et al.* [7]: 0.0732x/b + 0.332.

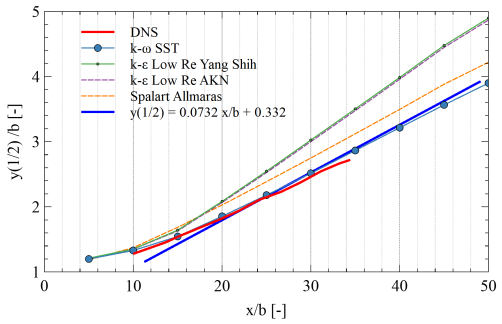

Figure 4: Growth rate for Low-Re modeling simulations along x.

The results obtained with $k-\omega$ SST and SA model show accurate values. The agreement is evident in Figure 4 - marked blue line and orange line - with an error associated of 6.8% and 1%. The one equation turbulence model (SA) was especially developed for aeronautics and wall-bounded flows and provides high accuracy as can be observed. The numerical error associated to the grid size was also inspected by a convergence study demonstrating the reliability of the results here displayed.

The situation of the jet being injected perfectly aligned with the wall is not applicable for the industrial process analysed due to construction constraints. Consequently, the jet faces a backward-facing step at the injection.

A numerical simulation with a step height equal

to 3 times the jet height was performed using SA turbulence model. The location of flow attachment depends on several conditions but the wall jet recovers the behaviour after the attachment. The results in Figure 5 display the dimensionless velocity profile at two different regions, $x/b = 30$ and $x/b = 45$, for simulations with and without backward-facing step. The figure shows the velocity profiles aligned between the two different situations (with or without step) and are very similar to the self-similar case for fully turbulent region.

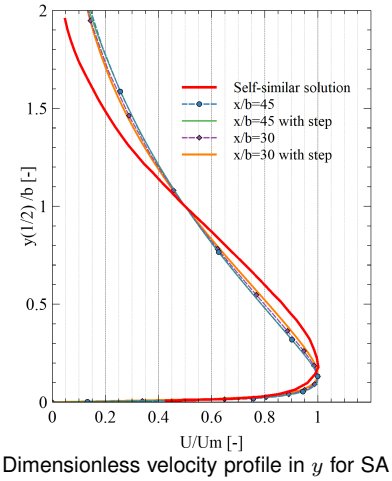

Figure 5: Dimensionless velocity profile in y for SA turbulence model.

The results inside the stagnation region are not focus of interest since the attachment is registered approximately at $x/b = 7$, which represents a small fraction when compared with the region that is going to be studied, $x/b = 120$ (around 5%).

3. Modeling, simulation, and cooling optimization of glass window

A simplified 1D model is considered to reduce the extremely high computational effort of the 3D numerical simulations. Numerical simulations of wall jets on a reduced geometrical model provided the heat transfer correlations associated to cooling on the glass window. The correlations and studies on cold wall jets were used in the 1D model for analysis purposes and for an energetic optimization of the optimal cooling conditions.

3.1. Development of 1D model

A one dimensional model of the window was developed to predict the thermal performance of the glass plate. Figure 6 represents schematically the situation inside an oven.

The glass thermal conductivity (k_t) is assumed constant along x because the difference of temperature inside the window is not significant. The 1D energy equation for the solid glass reads:

$$k_t \frac{\mathrm{d}^2 T}{\mathrm{d}x^2} = \frac{\mathrm{d}q_r}{\mathrm{d}x} \tag{7}$$

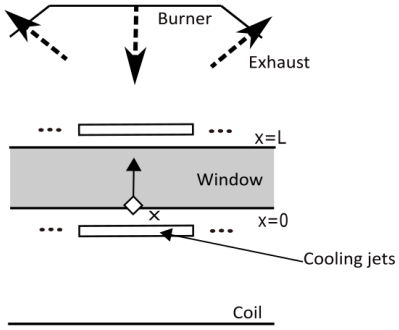

Figure 6: Schematic representation of curing furnace in a plane perpendicular to the coil.

Equation (7) was solved by finite differences and convective boundary conditions are applied at $x = 0$ and $x = L$.

$$-k_t \left.\frac{\mathrm{d}T}{\mathrm{d}x}\right|_{x=L} = h_{RBS}\left[T(L) - T_\infty^{RBS}\right] \tag{8a}$$

$$-k_t \left.\frac{\mathrm{d}T}{\mathrm{d}x}\right|_{x=0} = h_{COS}\left[T_\infty^{COS} - T(0)\right] \tag{8b}$$

h_{RBS} and h_{COS} are the convection coefficients of the surroundings environments at a certain temperature T_∞^{RBS} and T_∞^{COS}, respectively.

The divergence of radiative flux is directly related with the radiation intensity inside the medium. The radiation intensity can be computed according with the radiant transfer equation (RTE). The coupling between the two equations (RTE and energy balance) is non-linear due to the divergence of radiative flux depending on terms non-linear, such as T^4. An iterative procedure between energy equation and RTE is used on the development of the model. The local divergence of the radiative heat flux is given by a balance between the emitted intensity and incoming radiation (irradiation):

$$\left(\frac{\mathrm{d}q_r}{\mathrm{d}x}\right)_\lambda = k_\lambda(4\pi \times I_{b,\lambda}(x) - G_\lambda(x)) \tag{9}$$

The RTE represents the effects on the radiation intensity in a medium and comprising the simplifications for the case studied, the RTE can be rewritten in a simple form as:

$$\frac{\mathrm{d}I_\lambda}{\mathrm{d}\tau} + I_\lambda = I_{b,\lambda} \tag{10}$$

The direction of radiation is a parameter that needs to be considered. The solution method used in this work is the discrete ordinates method (DOM). The main idea of the model is the substitution of the integration of intensity in all directions by the summation of numerical quadrature of discrete different directions. This model relies on the angular discretisation since it is an approximation by summation. The non-gray model developed for this work is

not based on a black body but on a real body. The radiation of the boundary conditions is computed based on the radiosity (J). The radiosity represents the sum of the total radiant flux leaving the surface into the medium.

$$J_\lambda = \tau_\lambda G_\lambda + e_\lambda E_\lambda + \rho_\lambda H_\lambda \tag{11}$$

The surrounding surfaces define the radiation which reaches and penetrates the medium (G). The radiation is defined according with the surface temperature. The burner's surface temperature is unknown in opposite to the radiative efficiency/flux of the burner. An iterative procedure is added to the model to renew the temperature of the burner's surface according with the radiative flux balance.

Nusselt number commonly defines the convection coefficient as:

$$\overline{Nu} = \frac{\overline{h}L}{k_t} \tag{12}$$

where L is defined as a characteristic length.

The fluid flow and heat transfer conditions without cooling inside RBS can be approximated as an impinging jet onto a plate. The most adequate empirical correlation to the current model and to the conditions of the system is provided by the study of Martin [15] for a slot nozzle. The situation without cooling inside COS is approximated to a situation of natural convection.

The cooling jet is injected parallel to the window as a wall jet. The conditions of the system (backward-facing step at the entrance - 3 times the jet height and perpendicular wall at the end of the wall) demonstrate a very specific situation which correlations already studied become not suitable for the situation considered (see Figure 7). The strategy to obtain a valid correlation for the specific situations studied was simulate the case numerically. The geometrical model of RBS is simplified - half of one row of burners - due to symmetric conditions (see Figure 7). The case with cooling inside COS is similar but does not account for the burner's output.

The mathematical and physical models are the ones used in Section 2. The turbulence model of SA closes the RANS equations. The numerical model simulated prescribes the impingement conditions as nominal burner's output and varies the operating conditions of cooling (Reynolds number by manipulating the velocity and fixing the cooling gas temperature ($T_{COS/RBS}$)). An uniform temperature of the window is prescribed. The studies on heat transfer in wall jets considered an iso-thermal wall [11] and AbdulNour *et al.* [10] concluded that there is no difference by considering an iso-thermal or iso-flux surface. The heat transfer on the surface

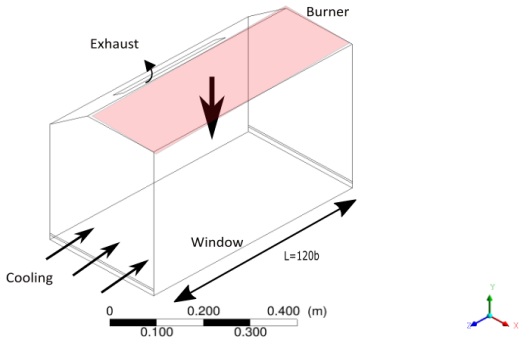

Figure 7: RBS geometric model of half battery of burners without the window.

of the window is then analyzed and the correlation can be then defined as literature reports for wall jet:

$$\overline{Nu} = f(Re) = C_1 \times Re^{C_2} \tag{13}$$

The properties are considered at an average temperature between inlet cooling gas temperature and window temperature.

The results show that the coefficient C_2 is almost equal to 0.8 for all numerical simulations. The results are consistent due to cooling behaviour being as wall jet - Equation (2). The coefficient C_1 is higher inside COS than RBS due to absence of impingement jet of burner's output, which reduces the heat transfer inside RBS.

Table 1: Coefficients for heat transfer correlation.

	RBS			COS		
	A	B	C	A	B	C
C_1	0.0048	0.0058	0.0037	0.0077	0.0088	0.0087
C_2	0.838	0.795	0.867	0.819	0.800	0.784

3.2. Results of parametric analysis

The 1D model developed was verified with literature solutions [16] and the model developed shows the expected behaviour for a conduction-radiation heat transfer study. The second verification was performed with data from a 2D model in a commercial software, ANSYS Fluent.

The results are displayed in Table 2 and show similar solutions for the two different cases. The absorbed thermal power ($\dot{q}$) and average window temperature ($\overline{T_w}$) increases when the thickness increases.

Table 2: Comparison of average window temperature and absorbed power between 1D model developed and 2D model in ANSYS Fluent for two window thicknesses.

Thickness	**1D**		**2D-Fluent**	
	$\overline{T_w}$ **[ºC]**	$\dot{q}$ **[**$\mathrm{kW/m^2}$**]**	$\overline{T_w}$ **[ºC]**	$\dot{q}$ **[**$\mathrm{kW/m^2}$**]**
2 mm	916.0	4.14	933	4.61
5 mm	1017.0	5.67	1000.0	5.78

The reference case without any cooling shows a non-linear temperature profile due to the influence of the radiation. The difference of temperature inside the medium is very small ($\Delta T = 1.04$ºC) due to the reduced thickness. The model computed the local divergence of radiative heat flux, graphically displayed in Figure 8. The absorption of energy ($\dot{q} = 3.71\mathrm{kW/m^2}$ - gray area in Figure 8) is the reason for the high temperatures of the medium ($\overline{T_w} = 889.2$ºC).

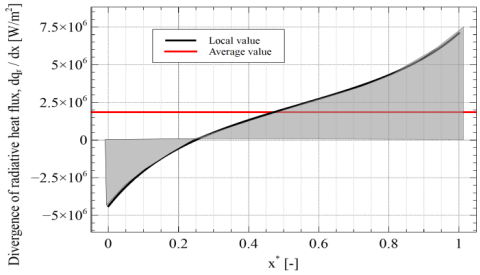

Figure 8: Divergence of radiative heat flux inside the window.

The parametric studies on the window thermal performance provided the conclusion that the increase of the thickness leads to an logarithmic increase of the temperature. For the same burner power, burner's radiative efficiency has a strong impact on the temperature of the window due to the high temperatures of the burner surface and coil temperature has a negligible effect due to the reduced temperature and emissivity.

The cooling is applied on the model developed taking into account heat transfer information derived from 3D numerical simulations of wall jets as previously described. The results with the cooling applied inside RBS on the 1D model are represented in Figure 9 by varying the cooling gas temperature and velocity.

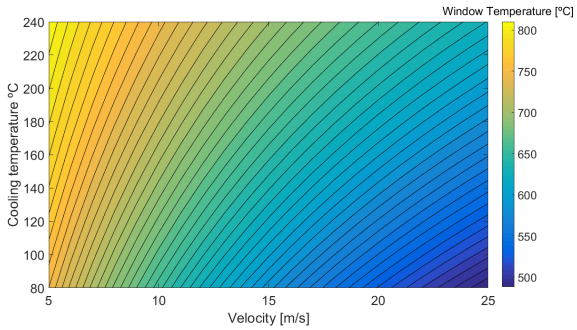

Figure 9: 2D contour plot of window temperature dependent of cooling velocity and temperature.

Figure 9 shows that the highest window temperatures are observed for lower (higher) cooling gas injection velocity (temperature) values. The results also demonstrate the high impact of cooling inside RBS on the reduction of the temperature. The temperature can be reduced 400ºC (889.2ºC without cooling to 506ºC) by a wall jet cooling with 25 m/s at 80ºC.

The nominal operating condition of cooling corresponds to 25 m/s at 80ºC in RBS and 12.5 m/s at 250ºC in COS. The results considering the effect of cooling inside COS and the combined effect are listed in Table 3. The cooling applied inside COS has a reduced impact on the reduction of window temperature due to the reduced velocity (v_{COS}=12.5 m/s) and the higher temperature of cooling (T_{COS}=250ºC).

Table 3: Window temperature as function of cooling inside RBS (v=25m/s and T=80ºC), COS (v=12.5m/s and T=250ºC) and combined situation.

Cooling	COS	RBS	Combined
$\overline{T_w}$ [ºC]	758.6	505.9	446.5

The results of average window temperature for the nominal operating condition considering the different cooling schemes are listed in Table 4. Cooling strategy A removes more heat from the window and strategy B registers 40ºC higher average window temperature than strategy A.

Table 4: Window temperature as function of type cooling.

Cooling strategies	A	B	C
$\overline{T_w}$ [ºC]	436.3	477.8	446.5

The numerical simulations provided information on the average convection coefficient, but also locally. The results of a numerical simulation for the same Reynolds number with different strategies inside RBS is represented in Figure 10. The regions with higher heat transfer convection coefficients match the zones near the injection due to the wall jet attachment. The region with lower heat transfer coefficient for strategy A and C is at the opposite wall due to the reduced velocities. Strategy C registers other region with lower heat transfer, at the middle of the window due to the effect of collision between opposite jets. The collision is not direct but affects the flow field and is responsible for the triangular shapes that can be observed. For strategy B, the jets collide directly at the middle (stagnation region) and the flow starts to develop on the normal direction. Cooling scheme B offers less variation of the convection coefficient (lower root mean square) by comparison with the other cooling strategies for all the Reynolds considered.

The previous information of heat transfer is accounted in the 1D model developed by regions of interest (see dashed black lines in Figure 10(a)). Due to non significantly change of local heat transfer on longitudinal direction for strategies A and B,

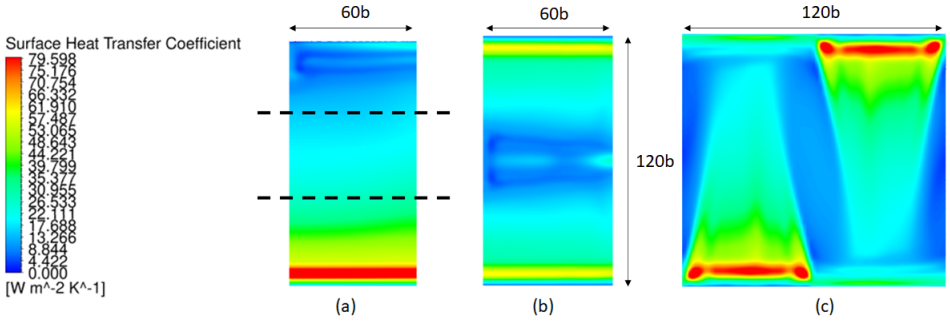

Figure 10: Local heat transfer coefficient at the window top surface (window-RBS interface) for different cooling schemes: (a) Scheme A; (b) Scheme B; and (c) Scheme C.

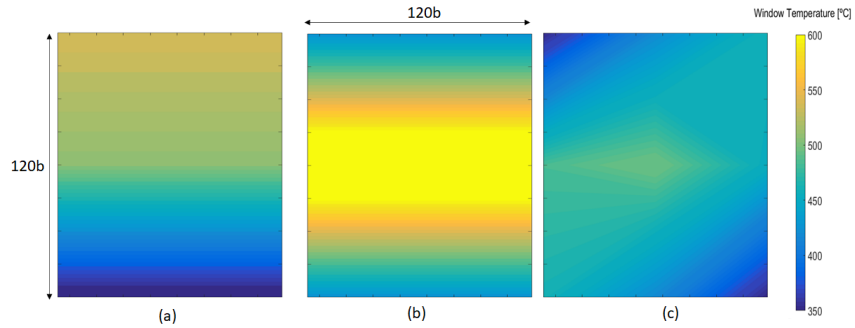

Figure 11: 3D window temperature results for nominal operating condition and different cooling schemes: (a) Scheme A; (b) Scheme B; and (c) Scheme C.

only 3 regions of interest were considered while for the strategy C, 9 regions of interest were considered due to the tri-dimensionality. The results for a nominal operating condition of cooling are displayed in Figure 11.

The results are qualitatively similar to the ones observed in Figure 10 since the cooling inside COS has a lower impact when compared with the cooling inside RBS. The maximum window temperatures for cooling B and C are at the middle of the plate since the stagnation/collision region inside RBS is the same as COS.

Cooling strategy C registers a lower maximum of temperature and less gradient of temperature than the other strategies. The advective effect of burner's output and the cooling angle injection brings negligible differences for the situations studied.

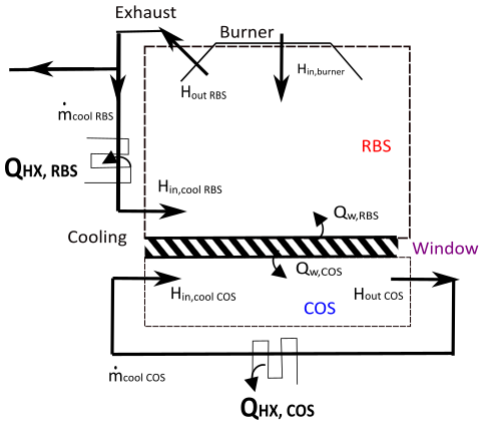

Figure 12: Schematic representation and energy balance of both sections.

3.3. Energetic optimization

The optimal situation matches the proper functioning (safety requirements) at the reduced energy cost. The energetic cost of the cooling operation is related to the thermal power of the two outside HX (see Figure 12).

$$Q_{HX} = \dot{m}_{cool} \times (h_{out} - h_{in,cool}) \qquad (14)$$

The total enthalpy of extracted fluid from environment (H_{outRBS} and H_{outCOS}) is dependent on the energy balance performed to the system. The difference of total enthalpy is equal to the heat removed from the window and gained by the system. The energy balance of the fluid for RBS reads:

$$H_{outRBS} - H_{in,coolRBS} - H_{in,burner} = Q_{w,RBS} \qquad (15)$$

The thermal power removed from the window by convection ($Q_{w,RBS/COS}$) is based on the 1D model developed.

The variables to optimize correspond to the cooling gas injection velocity and temperature for RBS (v_{RBS} and T_{RBS}) and COS (v_{COS} and T_{COS}), and the cooling strategy (five variables).

The optimized continuous variables are constrained in a domain with lower and upper bounds:

- 250ºC$< T_{COS} <$ 450ºC
- $5\mathrm{m/s} < v_{COS} < 25\mathrm{m/s}$
- 80ºC$< T_{RBS} <$ 450ºC
- $5\mathrm{m/s} < v_{RBS} < 25\mathrm{m/s}$

The atmosphere inside COS is loaded with solvent and due to condensation problems for temperatures below 250ºC, that was considered the lower limit of cooling gas temperature.

The optimal solution is not exclusively constrained by the provided solution space (domain limits for each optimized variable). The optimal solution is also constrained by a maximum temperature and a maximum temperature gradient that must be below the corresponding critical values:

- $T_{max,w} < T_{critical}$
- $\Delta T_w < \Delta T_{critical}$

These constrains are non-linear but are function of the optimised variables according with the 1D model developed.

The optimization toolbox of MATLAB was used to solve the optimization formulation previously presented. The solver method used was the initial-point algorithm and a search with multiple initial points (10) is used to dissipate the errors. The genetic algorithm resulted in a high computational effort due to a non-linear constrained based on the model developed.

The cooling power demand increases when there is a need of a lower maximum temperature. The optimization shows that the use of the HX inside COS is more relevant in energetic purposes since there is no mixing with a hot fluid from the burner's output. The choice of the best cooling scheme is not universal because it depends on project requirements.

For maximum temperatures below 400ºC, the system dictates that the operation is not feasible.

4. 3D numerical simulations

The 1D model developed offers the optimal response to the user on the thermal control of the window but has limitations and assumptions, by not considering enclosure walls. The modeling and simulation of the full curing furnace considering the different effects is important to the analysis and verification of the work performed.

Fluent code was used to discretize the physical domain and to solve the set of 3D governing equations for mass, momentum, energy conservation in steady-state form, and also the chemical species transport equation for O_2, CO_2, H_2O, N_2 and an effective solvent species. The fluid was defined as a gas mixture and modeled according to the mixture average formalism. The properties related to species were defined according with Fluent database, considering temperature dependence with Sutherland's law. The ideal gas model was considered for the evaluation of the fluid density. The $k-\epsilon$ turbulence model was applied to provide closure for the RANS equations. The radiative heat transfer exchanges in the full 3D domain were taken into account through the application of the DOM with an S6 angular discretisation. The numerical model resulted in a mesh of 6.18 million cells in total. The refinement and low-Re modeling near the window was not possible due to the unaffordable computational cost.

The numerical simulations are conducted for a nominal operating condition of 600 kW with the first three batteries of burners active. At the burner's outlet section, temperature and velocity values are prescribed for the flue gas stream and a fixed temperature value is applied on the corresponding surface area – radiative contribution. A pressure-outlet boundary condition stating atmospheric pressure conditions was applied at the flue gas extraction sections. The surface walls were defined with an emissivity equal to 0.8.

The solvent species evaporation was prescribed as an uniform mass source along the metal strip inside the COS (7.5×10^{-3} kg/s). The metal strip with a velocity equal to 0.5 m/s has a linear increase of the temperature inside the COS from 25ºC to 250ºC.

The situation without any cooling system applied underneath and above the window is herein analyzed and the average window temperature is 946 ºC. The second investigation is conducted with the system of cooling applied underneath the window in an alternated scheme as the strategy C. The flow pattern removes heat from the window in a triangular shape due to the influence of the opposite flow, resulting in a temperature distribution as the Figure 13. This effect is in agreement with already observed for the convection coefficient (Figure 10).

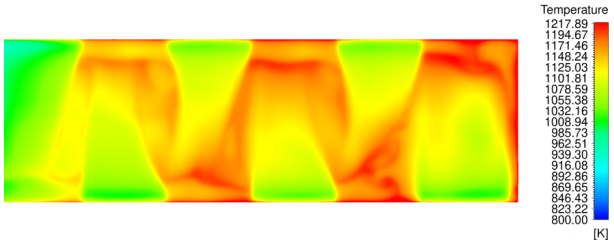

Figure 13: Window temperature distribution with cooling inside COS.

Figure 14 shows the window temperature distribution inside the window for the situation with com-

bined cooling. The distribution of temperatures is not uniform in any direction. The cooling applied inside RBS faces a step at the injection which is 10 times higher than the jet height ($h = 10b$).

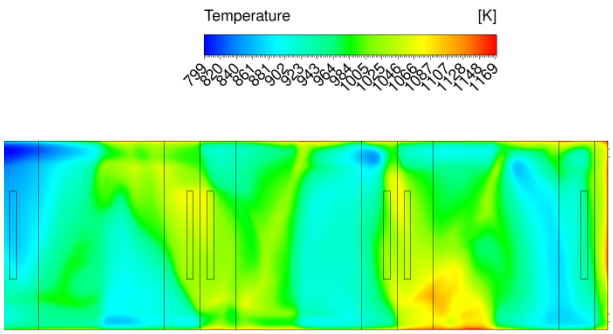

Figure 14: Window temperature distribution with combined cooling.

The radiative flux in burner's output is computed as 181.60 kW, which is in agreement with a radiative efficiency equal to 0.3. The walls inside RBS have a radiative gain corresponding to 35.9 kW (19.74%) and the window absorbs 23.4 kW (12.86%). The remaining part of the radiative flux is transferred to the COS and absorbed by the coil. The coils absorbs 103.6 kW (57%) of radiative energy.

The analysis of the full furnace allows a comparison with the results obtained with the 1D model developed. Table 5 presents the average window temperature for different situations.

Table 5: Comparison of average window temperature between 3D models and 1D model.

Model	No cooling	COS	RBS	Combined
3D - $\overline{T_w}$ [ºC]	926	830	732	683
1D - $\overline{T_w}$ [ºC]	889	758	502	446

The results show similar values for the situation without cooling, with a difference of only 30ºC. The numerical simulations for the cases with cooling register higher differences. The simulations with cooling inside RBS demonstrate a higher difference due to the difference on step height considered. The same effect of combined cooling is verified for both models, a reduction of around 50ºC when compared with the cooling applied only in RBS.

For the operating conditions under consideration, the extracted gas temperature in RBS predicted by the 1D model and the 3D model is approximately equal to 698ºC and 803ºC, respectively. The higher 3D model exhaust temperature is explained by the role of furnace walls: furnace walls are neglected in the 1D model but not in the 3D model. Furnace walls are responsible for transferring a net radiative power to the surrounding fluid by convection heat transfer.

The importance of heat losses through the furnace walls is investigated considering the wall insulation material and thickness. The investigation compares the overall performance for different thicknesses with the adiabatic case. An overall heat transfer coefficient was calculated and then implemented in the simulation. The heat losses reduce in a proportional way with the increase of the thickness. The losses correspond to 1% of the total power input from the burners for the more realistic situation and therefore the system is almost adiabatic.

5. Conclusions

The present work simulates in 1D, 2D, and 3D models the heat transfer in a curing furnace by IR radiative energy exchange. The analysis of the curing furnace identified high temperatures inside the glass partition due to its absorption to radiation. The cooling system is applied as a cold wall jet.

Different turbulent models in wall jets were investigated numerically, where k-w SST and SA models with low-Re modeling proved to have higher accuracy. Due to construction constraints, the cold wall jets face a backward step at the entrance and the numerical studies demonstrated that after the flow reattachment of the plate, the flow behaves as a typical wall jet.

A 1D model of the window using the discrete ordinates method was developed to predict the thermal behaviour of the glass. The model predicts that glass window registers high temperatures for the case without cooling (889ºC). An increase of the thickness will result in a logarithmic increase of the absorption and consequently, window temperature.

Numerical simulations were performed to obtain the heat transfer correlations associated to wall jet cooling for the specific cases studied. This information is integrated in the 1D model to an extensive analysis. The cooling system demonstrated a high impact on the reduction of the temperature.

Cooling inside COS (underneath the glass) has a lower effect than cooling inside RBS (above the window) for the nominal operating condition, as a result of the reduced mass flow rate and high cooling gas temperature defined at the injection of COS.

Three different cooling strategies are analyzed and compared. The 1D model developed is used not just in an average evaluation but in local regions to provide the temperature gradient. Cooling from two-sides leads to less heat removed from the window and higher temperature gradients due to the stagnation region at the middle of the plate. There is no significant difference on the total heat

removed from the window by considering cooling from one-side or in alternated scheme.

The burner's output has a negligible effect on cooling inside RBS due to the reduced velocity ratio and the injection of a cold wall jet with a certain angle brings negligible differences.

The optimization procedure leads to the optimal cooling conditions for certain safety requirements (maximum window temperature and gradient of temperature). The demand of cooling power increases when there is a need of a lower maximum temperature. The optimization shows that the use of the heat exchanger inside COS is more relevant for energetic purposes since there is no hot fluid from burner's output as in RBS. The optimization does not dictate a universal best choice for the scheme of cooling because that depends on the safety requirements. An alternated cooling scheme is a more efficient choice but presents higher thermal gradients than cooling from one-side.

The numerical simulations to the full curing furnace demonstrated similar conclusions and results obtained with the 1D model developed. The results also identified the high window temperature for the situation without cooling (929ºC). The energy balances were verified and the system can be considered as adiabatic due to the wall constituent materials and dimensions. However, the radiative gain of the walls matches with a convection heat loss to the fluid. This effect is not negligible and is not considered in the 1D model, justifying the differences observed between 1D and 3D model.

References

[1] L. Lori, A. Tamba, F. Deflorian, L. Fedrizzi, and P. L. Bonora. Stainless steel as new substrate for coil coating. *Progress in Organic Coatings*, 27(1-4):17–23, 1996.

[2] Tore Kolås, Arne Røyset, Mathieu Grandcolas, and Anica Lacau. Solar energy materials and solar cells cool coatings with high near infrared transmittance for coil coated aluminium. *Solar Energy Materials and Solar Cells*, 196(December 2018):94–104, 2019.

[3] Energy Efficient Coil Coating Process, European Project, https://www.spire2030.eu/ecco.

[4] M. B. Glauert. The wall jet. *Journal of Fluid Mechanics*, 1(06):625, 1956.

[5] B E Launder and W Rodi. The turbulent wall jet measurements and modeling. *Annual Review of Fluid Mechanics*, 15(1):429–459, 1983.

[6] William K. George, Hans Abrahamsson, Jan Eriksson, Rolf I. Karlsson, Lennart Lofdahl, and Martin Wosnik. A similarity theory for the turbulent plane wall jet without external stream. *Journal of Fluid Mechanics*, 425:367–411, 2000.

[7] H. Abrahamsson, B. Johansson, and L. Lofdahl. A turbulent plane two-dimensional wall-jet in a quiescent surrounding. *Eur. J. Mech. B/Fluids 13*, pages 533–556, 1994.

[8] J. Persson J. G. Eriksson, R. I. Karlsson. An experimental study of a plane turbulent wall jet using LDA. 25:50–60, 1998.

[9] T. Dakos, C. A. Verriopoulos, and M. M. Gibson. Turbulent flow with heat transfer in plane and curved wall jets. *Journal of Fluid Mechanics*, 145(-1):339, 1984.

[10] R. S. AbdulNour, K. Willenborg, J. J. McGrath, J. F. Foss, and B. S. AbdulNour. Measurements of the convection heat transfer coefficient for a planar wall jet: Uniform temperature and uniform heat flux boundary conditions. *Experimental Thermal and Fluid Science*, 22(3-4):123–131, 2000.

[11] Iftekhar Z. Naqavi, James C. Tyacke, and Paul G. Tucker. A numerical study of a plane wall jet with heat transfer. *International Journal of Heat and Fluid Flow*, 63:99–107, 2017.

[12] J. Cahit Akfirat. Transfer of heat from an isothermal flat plate to a two-dimensional wall jet. In *Proceeding of International Heat Transfer Conference 3*, pages 274–279, Connecticut, 1966.

[13] B. A. Kader and A. M. Yaglom. Heat and mass transfer laws for fully turbulent wall flows. *International Journal of Heat and Mass Transfer*, 15(12):2329–2351, 1972.

[14] Mohammad Mahmoudi, David Nobes, and Brian Fleck. An experiment design for measuring the velocity field of a round wall jet in counter-flow. *International Journal of Mechanical Engineering and Mechatronics*, 2014.

[15] Holger Martin. Heat and mass transfer between impinging gas jets and solid surfaces. *Advances in Heat Transfer*, 13(C):1–60, 1977.

[16] Prabal Talukdar and Subhash C Mishra. Analysis of conduction-radiation problem in absorbing, emitting and anisotropically scattering media using the collapsed dimension method. *International Journal of Heat and Mass Transfer*, 45(10):2159–2168, 2002.